A comparison of stabilized least-squares imaging conditions for wave-equation migration

Bruno D. Amaro[1], Jörg Schleicher[2], Amélia Novais[2] and Jessé C. Costa[3] .

[1] University of Campinas - UNICAMP, Dept. of Applied Mathematics, Campinas, Brazil.

[2] University of Campinas - UNICAMP, Dept. of Applied Mathematics, Campinas, Brazil; INCT-GP.

[3] Federal University of Pará - UFPA - Faculty of Geophysics, Belém, Brazil; INCT-GP.

Abstract

In seismic migration, after the wave propagation process, an important step to obtain a migrated image is the application of an image condition. Several alternative forms of imaging conditions have emerged in the recent past that are evaluated by the quality of the output amplitudes and artifacts produced. In this paper, we present new stabilized least-squares image conditions and compare them to previously proposed forms. Our numerical experiments on the Marmousi data set show that they produce satisfactory results.

Introduction

The theoretical imaging condition of Claerbout (1971) consists of dividing the upcoming wavefield by the downgoing wavefields in the frequency domain and summing the result over all frequencies and sources used in the process. Because we do not know the real reflector position, this division must be carried out at all image points. This can cause some instability during the process, because the downgoing wavefield is zero in points off the reflector. To try solve this problem, different techniques have been proposed, the first being a crosscorrelation instead of the theoretically required deconvolution (Claerbout, 1971). However, this procedure destroys the amplitude information contained in the data. More recent attempts to approximate the deconvolutional imaging condition try to avoid this to recover the reflection coefficient at the image point (Valenciano and Biondi, 2003; Guitton et al., 2007; Schleicher et al., 2008; Vivas et al., 2009).

The reflection coefficient can be estimated by a least-squares procedure (Arienti et al., 2002). Its solution consists of dividing the crosscorrelation of the upcoming and downgoing wavefields by the autocorrelation of the downgoing wavefield. To stabilize this solution, Schleicher et al. (2008) proposed two possible modifications: to add a small constant to the autocorrelation of the downgoing wavefield in the denominator, or to smooth this denominator before the division, modifying the original idea of Guitton et al. (2007) of smoothing the absolute value of the downgoing wavefield in the denominator.

Based on the same fundamental principles, Vivas et al. (2009) proposed a stabilized least-squares imaging condition that, different from the other conditions, started at a least-squares imaging condition that used the sum over all sources before the division of the wavefields. To stabilize the division, Vivas et al. (2009) replace the denominator at points of low value by a proportion of its average value.

In this paper we combine the ideas of Vivas et al.'s stabilized least-squares condition with the stabilization techniques of Schleicher et al. (2008). We test the so-created new stabilized least-squares imaging conditions on the Marmousi data and compare them to the versions from the literature.

Theory

Wave-equation migration tries to undo the effects that the wave propagation had on the surface data $Q(x_r, y_r; \omega)$ recorded at the receiver position $\mathbf{x}_r = (x_r, y_r, z = 0)$. These effects are generally approximately described by the acoustic wave equation which, after Fourier transform, is given by

$$\left(\frac{\omega^2}{\upsilon^2(\mathbf{x})} + \frac{\partial^2}{\partial z^2} + \Delta\right) P(\mathbf{x}, \omega) = -\delta(\mathbf{x} - \mathbf{x}_s), \qquad (1)$$

where $P(\mathbf{x}, \omega)$ is the wavefield being propagated at a point $\mathbf{x} = (x, y, z)$, $\upsilon(\mathbf{x})$ is the wavefield velocity, $\mathbf{x}_s$ denotes the source position, and $\Delta = \frac{\partial^2}{\partial x^2} + \frac{\partial^2}{\partial y^2}$. The solution of this equation at $\mathbf{x}_r$ must be equal the recorded surface data $Q(x_r, y_r; \omega)$, i.e, the wavefield $P(x_r, y_r, z = 0; \omega)$ must satisfy the boundary condition

$$P(x_r, y_r, z = 0; \omega) = Q(x_r, y_r; \omega). \qquad (2)$$

To migrate the data $Q(x_r, y_r; \omega)$ means to map this solution into depth. For this purpose, equation (1) is decomposed into two one-way equations given by

$$\left(\frac{\partial}{\partial z} - i\frac{\omega}{\upsilon(\mathbf{x})}\sqrt{1 + \frac{\upsilon^2(\mathbf{x})}{\omega^2}\Delta}\right) P_U(\mathbf{x}, \omega) = 0 \qquad (3)$$

with initial condition $P_U(x, y, z = 0, \omega) = Q(x, y; \omega)$ and

$$\left(\frac{\partial}{\partial z} + i\frac{\omega}{\upsilon(\mathbf{x})}\sqrt{1 + \frac{\upsilon^2(\mathbf{x})}{\omega^2}\Delta}\right) P_D(\mathbf{x}, \omega) = 0 \qquad (4)$$

with initial condition $P_D(x, y, z = 0, \omega) = \delta(\mathbf{x} - \mathbf{x}_s)$, where P_D e P_U represent the downgoing and upcoming wavefields, respectively

We use these one-way wave equations to simulate the wave propagation from initial conditions at $z = 0$ into the underground, where the downgoing wavefields are propagated forward from $t = 0$ and the upcoming wavefields are propagated backward from $t = t_{max}$.

After the propagation step, an imaging condition must be applied to obtain the final migrated image. Theoretically, the correct imaging condition is the deconvolution (division in the frequency domain) of both wavefields at reflector depth to recover the reflection coefficient as the amplitude of the obtained image (Claerbout, 1971)

$$R(\mathbf{x}) = \sum_{j=1}^{N_\omega} \frac{P_U(\mathbf{x},\omega_j)}{P_D(\mathbf{x},\omega_j)}, \tag{5}$$

where N_ω is the number of frequency used in the process. Because the reflector position is unknown, this division must be carried out at all image points. This implies a certain instability during the process, because the downgoing wavefield, which is in the denominator of equation (5), will be zero at points that are not part of a reflector. For this reason, it is necessary to find a way to stabilize the imaging process. Some ideas are described below.

Imaging conditions

Crosscorrelation

The simplest and most stable imaging condition is the one proposed by Claerbout (1971). It uses a simple crosscorrelation of the upcoming and downgoing wavefields, i.e., a convolution of the upcoming wavefield with the complex conjugate of the downgoing wavefield,

$$R_c(\mathbf{x}) = \sum_{j=1}^{N_\omega} P_U(\mathbf{x},\omega_j) P_D^*(\mathbf{x},\omega_j), \tag{6}$$

where the asterisk denotes the complex conjugate.

This condition is obtained as a simplification of the expression

$$R(\mathbf{x}) = \sum_{j=1}^{N_\omega} \frac{P_U(\mathbf{x},\omega_j) P_D^*(\mathbf{x},\omega_j)}{P_D(\mathbf{x},\omega_j) P_D^*(\mathbf{x},\omega_j)}, \tag{7}$$

which is obtained from equation (5) by multiplication of numerator and denominator with $P_D^*(\mathbf{x},\omega_j)$, an operation which moves all phase operations in the numerator and makes the denominator real.

Equation (7) does not solve the problem of division by zero. The advantage is that now the denominator is only a scale factor that no longer contains any phase information, i.e., information about the reflector position. Thus, if our interest is to know the reflector position with no amplitude preservation, the denominator can be omitted, leading to imaging condition (6).

We can check that the imaging condition 6 does not need any division. Thus the instability problems do not occur. This characteristic, along the fact that no one has given importance of amplitudes information in the application of seismic migration, made this imaging condition has become the most used in practice.

Division by autocorrelation

Another imaging condition, addressed by Schleicher et al. (2008), is given by

$$R_{da}(\mathbf{x}) = \frac{\sum_{j=1}^{N_\omega} P_U(\mathbf{x},\omega_j) P_D^*(\mathbf{x},\omega_j)}{\sum_{j=1}^{N_\omega} P_D(\mathbf{x},\omega_j) P_D^*(\mathbf{x},\omega_j)}. \tag{8}$$

This imaging condition is also known as illumination compensation and can be interpreted as the result of a least-squares inversion of the equation $P_U(\mathbf{x}) = R(\mathbf{x}) P_D(\mathbf{x})$. Moreover, it is roughly equivalent to imaging condition (6). The reason is that in ray-theoretical approximation, $\sum_{j=1}^{N_\omega} P_D(\mathbf{x},\omega_j) P_D^*(\mathbf{x},\omega_j) \approx A_d^2$, where A_d represents the amplitude of P_D. Thus, equation (8) is approximately equivalent to

$$R(\mathbf{x}) = \sum_{j=1}^{N_\omega} \frac{P_U(\mathbf{x},\omega_j) P_D^*(\mathbf{x},\omega_j)}{P_D(\mathbf{x},\omega_j) P_D^*(\mathbf{x},\omega_j)} \approx \frac{1}{A_d^2} \sum_{j=1}^{N_\omega} P_U(\mathbf{x},\omega_j) P_D^*(\mathbf{x},\omega_j). \tag{9}$$

Other slightly modified forms of imaging condition (8) were also addressed by Schleicher et al. (2008). These are

$$R_{ad}(\mathbf{x}) = \frac{\sum_{j=1}^{N_\omega} P_U(\mathbf{x},\omega_j) P_D^*(\mathbf{x},\omega_j)}{\sum_{j=1}^{N_\omega} P_D(\mathbf{x},\omega_j) P_D^*(\mathbf{x},\omega_j) + \varepsilon} \tag{10}$$

where

$$\varepsilon = \varepsilon(z) = \max\{\alpha, \lambda \max_{x,y}(|D(\mathbf{x},\omega)|)\} \tag{11}$$

with $D(\mathbf{x},\omega)$ denoting the denominator in equation (8) and λ and α being parameters that keep ε from getting too small, and

$$R_{as}(\mathbf{x}) = \frac{\sum_{j=1}^{N_\omega} P_U(\mathbf{x},\omega_j) P_D^*(\mathbf{x},\omega_j)}{\ll \sum_{j=1}^{N_\omega} P_D(\mathbf{x},\omega_j) P_D^*(\mathbf{x},\omega_j) \gg}, \tag{12}$$

where

$$\ll Q(x_i, y_k, z, \omega) \gg = \sum_{l=i-n_x}^{i+n_x} \sum_{m=k-n_y}^{k+n_y} Q(x_l, y_m, z, \omega) \tag{13}$$

represents the smoothing operator addressed in Guitton et al. (2007), with n_x and n_y denoting the smoothing windows sizes in the x and y directions, respectively.

Stabilized least squares

Unlike the imaging conditions discussed above, Vivas et al. (2009) proposed an alternative least-squares imaging condition that computes, for each source, frequency and depth level, the average over the horizontal coordinates of the downgoing wavefield. Wherever the downgoing energy is below a certain threshold given by a fraction of this mean value, it is replaced by the threshold value. The

stabilized value of the denominator is then obtained by a final sum over frequency and sources, for each spatial position. Mathematically, in this formulation, we start with the following imaging condition

$$R_{ls}(\mathbf{x}) = \frac{\sum_{\mathbf{x}_s}\sum_{j=1}^{N_\omega} P_U(\mathbf{x}_s,\mathbf{x},\omega_j)P_D^*(\mathbf{x}_s,\mathbf{x},\omega_j)}{\sum_{\mathbf{x}_s}\sum_{j=1}^{N_\omega}|P_D(\mathbf{x}_s,\mathbf{x},\omega_j)|^2}. \qquad (14)$$

The average of the energy of the downgoing wavefield is given by

$$|P_D(\mathbf{x}_s,\mathbf{x},\omega)|^2_{av} = \frac{1}{N_x}\frac{1}{N_y}\sum_x\sum_y |P_D(\mathbf{x}_s,x,y,z,\omega)|^2 \qquad (15)$$

where N_x e N_y are the number of points of the image in the x and y directions.

Then, we replace the energy flux of the downgoing wavefield in equation (14) by its stabilized value $|P_D(\mathbf{x}_s,\mathbf{x},\omega)|^2_{st} =$

$$\begin{cases} |P_D(\mathbf{x}_s,\mathbf{x},\omega)|^2 & \text{if} \quad |P_D(\mathbf{x}_s,\mathbf{x},\omega)|^2 > \beta|P_D(\mathbf{x}_s,\mathbf{x},\omega)|^2_{av} \\ \beta|P_D(\mathbf{x}_s,\mathbf{x},\omega)|^2_{av} & \text{if} \quad |P_D(\mathbf{x}_s,\mathbf{x},\omega)|^2 \le \beta|P_D(\mathbf{x}_s,\mathbf{x},\omega)|^2_{av}, \end{cases} \qquad (16)$$

with β an arbitrary positive constant, and we get the stabilized least-squares imaging condition given by

$$R_{sls}(\mathbf{x}) = \frac{\sum_{\mathbf{x}_s}\sum_{j=1}^{N_\omega} P_U(\mathbf{x}_s,\mathbf{x},\omega_j)P_D^*(\mathbf{x}_s,\mathbf{x},\omega_j)}{\sum_{\mathbf{x}_s}\sum_{j=1}^{N_\omega}|P_D(\mathbf{x}_s,\mathbf{x},\omega_j)|^2_{st}}. \qquad (17)$$

The main difference to the previous imaging conditions lies in the fact that the sum over all source positions is carried out before the division of the wavefields. In the previous imaging conditions, the sum over all sources is carried out at the end, i.e., after the division of the wavefields.

Combining the stabilization ideas of the previous imaging conditions with the one from the last condition (**??**), we propose the alternative conditions

$$R_{sd}(\mathbf{x}) = \frac{\sum_{\mathbf{x}_s}\sum_{j=1}^{N_\omega} P_U(\mathbf{x}_s,\mathbf{x},\omega_j)P_D^*(\mathbf{x}_s,\mathbf{x},\omega_j)}{\sum_{\mathbf{x}_s}\sum_{j=1}^{N_\omega}|P_D(\mathbf{x}_s,\mathbf{x},\omega_j)|^2+\varepsilon}, \qquad (18)$$

and

$$R_{ss}(\mathbf{x}) = \frac{\sum_{\mathbf{x}_s}\sum_{j=1}^{N_\omega} P_U(\mathbf{x}_s,\mathbf{x},\omega_j)P_D^*(\mathbf{x}_s,\mathbf{x},\omega_j)}{\ll\sum_{\mathbf{x}_s}\sum_{j=1}^{N_\omega}|P_D(\mathbf{x}_s,\mathbf{x},\omega_j)|^2\gg}, \qquad (19)$$

where the additive constant ε and the smoothing operator "$\ll \quad \gg$" are given by equations (11) and (13), respectively.

Numerical tests

To test the quality of the proposed imaging conditions, we applied them to Marmousi data set by Versteeg (1994). The migration used was *Phase Shift Plus Interpolation* (PSPI) migration with ten reference velocities chosen according to the maximum entropy criterion of Bagaini et al. (1995). For simplicity, all numerical experiments were carried out in two dimensions. In all cases, we used the same migration technique and the true velocity distribution of the Marmousi model, changing only the imaging conditions. Thus all differences between the images below depend exclusively on the imaging conditions used.

Crosscorrelation

Figure 1 shows the result of condition R_c. This imaging condition is considered a benchmark, because it is the most stable imaging condition known, and it is widely used in practice. All other imaging conditions are not supposed to degrade the image quality in comparison with this one.

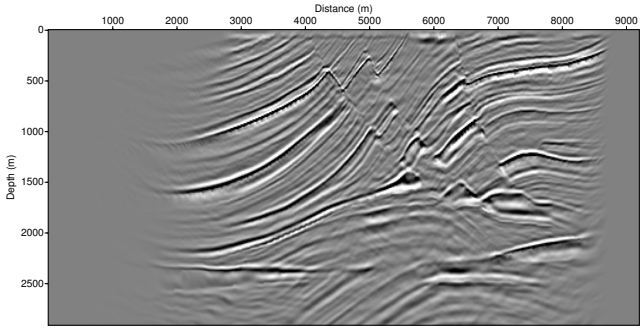

Figure 1: Marmousi data migrated using the crosscorrelation imaging condition R_c (equation 6).

Division by autocorrelation

Figures 2 and 3 show the results of imaging conditions R_{ad} e R_{as} given by equations (10) and (12), respectively. For the additive constant ε we used $\lambda = 0.05$ and $\alpha = 10^{-6}$ (equation 11). Although the overal quality of both images is similar, imaging condition R_{as} is better in the upper part of the image and R_{ad} produces a clearer image in the lower part. Some migration artifacts remain in both images. The stronger ones can be observed in Figure 3.

Stabilized least squares

The image in Figures 4, 5, 6, and 7 show the results of conditions R_{ls}, R_{sls}, R_{sd} and R_{ss} given by equations (14), (17), (18) and (19), respectively. In equation (17) we used $\beta = 1$ and in equation (18) we used $\varepsilon = 10^{-6}$. As a first advantage of these least-squares conditions, we note that in both figures, the images extend much further into the boundary zone than in Figures 2 and 3.

After a more detailed inspection of the image in Figure 4, we see the presence of artifacts near the surface, a problem solved by imaging condition R_{sls} (Figure 5). However, these artifacts appear only in the boundary region of the image, where the available data are

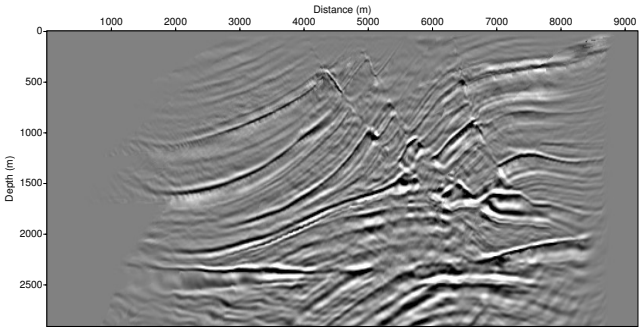

Figure 2: Marmousi data migrated using the imaging condition R_{ad} (equation 10) with $\lambda = 0.05$ and $\alpha = 10^{-6}$.

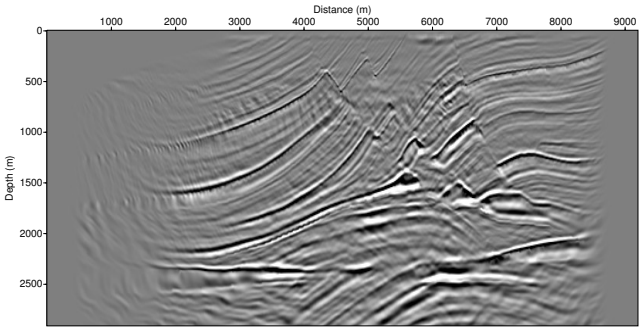

Figure 3: Marmousi data migrated using the imaging condition R_{as} (equation 12) with window size $n_x = 100$.

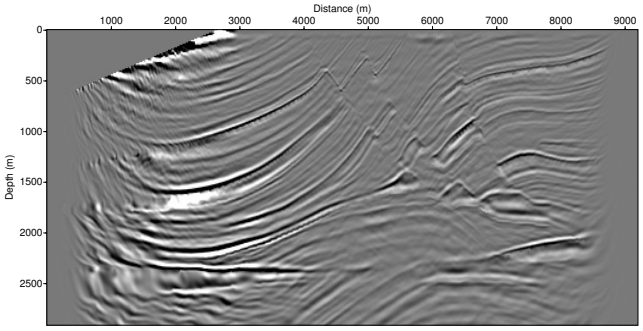

Figure 4: Marmousi data migrated using the imaging condition R_{ls} (equation 14).

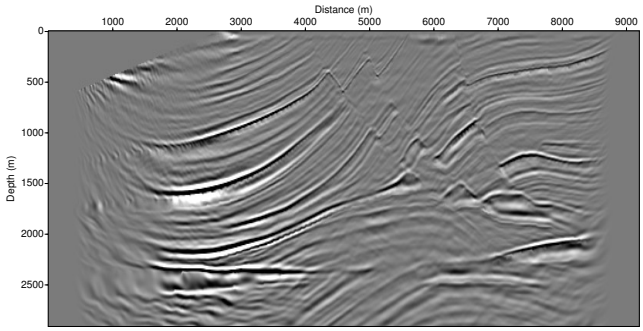

Figure 5: Marmousi data migrated using the imaging condition R_{sls} (equation 17) with $\beta = 1$ in equation 16.

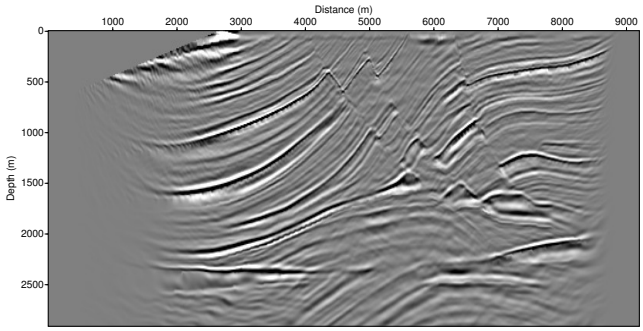

Figure 6: Marmousi data migrated using the imaging condition R_{sd} (equation 18) with $\varepsilon = 10^{-6}$.

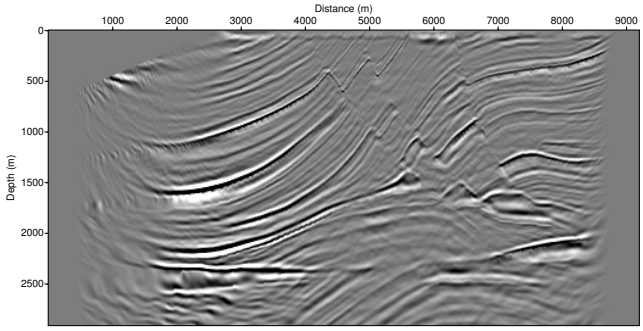

Figure 7: Marmousi data migrated using the imaging condition R_{ss} (equation 19).

insufficient anyway. In both cases the artifacts persist to a depth of about 1500 m. The amplitudes in Figuress 4 and 5 are visibly reduced as compared to Figures 2 and 3.

The fact that the least-squares and stabilized least-squares imaging conditions (equations 14 and 17) have produced good results with different artifacts being removed than in the case of conditions (10) and (12) has motivated us to combine the respective types of stabilization, hoping that this combination can help to remove all observed migration artifacts. The results of the combined imaging conditions (18) and (19) are shown in Figures 6 and 7.

Both imaging conditions R_{sd} e R_{ss} (Figures 6 and 7) show a considerable improvement over the imaging condition R_{sls} (Figure 5). In the case of condition R_{sd} we can see a clearer image in the upper part as compared to R_{ss}. Overall, very few migration artifacts are visible in both images, but particularly so in Figures 6. We recognize that the extension into the boundary zone achieved by conditions

R_{ls} and R_{sls} is also achieved by the present conditions. Note also that the amplitudes in both images are less affected by the stabilization than those in Figures 4 and 5 and closer to those in Figures 2 and 3. Therefore we can conclude that both new stabilization methods acted positively, creating satisfactory results that combined the advantages of the conditions discussed by Schleicher et al. (2008) and Vivas et al. (2009).

The general observation from the overall comparison of Figures 2 to 7 is that imaging condition R_{sd} (equation 18) produced the best image (Figure 6) with the least migration artifacts and the least affected migration amplitudes. Its image quality comes very close to the one of the simple crosscorrelation imaging condition R_c (Figure 1) of equation (6).

Conclusions

When the amplitudes of a migrated image are to be interpreted, the standard crosscorrelation imaging condition of Claerbout (1971) cannot be used since it destroys the amplitude information. This is particularly important, if true-amplitude algorithms are used to correct for geometrical-spreading effects in heterogeneous media. Several techniques to preserve the meaning of migrated amplitudes as proportional to the reflection coefficient at the image point while avoiding problems with divisions by near-zero values have been discussed in the recent past (Valenciano and Biondi, 2003; Guitton et al., 2007; Schleicher et al., 2008; Vivas et al., 2009). In this paper, we have combined ideas of several of them to come up with two new stabilization criteria for least-squares imaging conditions. These stabilized least-squares imaging conditions help to avoid instability problems in the migrated image by summing over all sources before smoothing the denominator or adding a given constant.

Tests on the Marmousi data indicated that the new stabilized least-squares imaging conditions can help to reduce migration artifacts. In our experiments, the new conditions resulted in superior image quality as compared to other recently proposed imaging conditions, both with regard to migration artifacts and to migrated amplitudes.

Acknowledgments

We would like to thank the Coordenação de Aperfeiçoamento de Pessoal de Nível Superior (CAPES, Brazil), the Conselho Nacional de Desenvolvimento Científico e Tecnológico (CNPq), as well as Petrobras and the sponsors of the Wave Inversion Technology (WIT) consortium for providing financial support for this research.

References

Arienti, M. T., E. Bonomi, G. Cardone, and L. Cazzola, 2002, Amplitude-preserving Monte Carlo 3D prestack migration: 64th EAGE Conference and Exhibition, Expanded Abstracts, EAGE, B09:1–4.

Bagaini, C., E. Bonomi, and E. Pieroni, 1995, Split convolutional approach to 3D depth extrapolation: 65th Annual International Meeting, SEG, Expanded Abstracts, 195-198

Claerbout, J. F., 1971, Toward a unified theory of reflector mapping: Geopshysics, **36**, 467-481.

Gazdag, J., 1978, Wave equation migration with phase-shift method: Geopshysics, **43**, 1342-1351.

Gazdag, J., and Sguazzero P., 1984, Migration os seismic data by phase shift plus interpolation: Geophysics, **49**, 124-131.

Guitton, A., A. Valenciano, D. Bevc, and J. Claerbout, 2007, Smoothing imaging condition for shot profile migration: Geophysics, **72**, no. 3, S149-S154.

Schleicher, J., Costa, J. C., and Novais, A., 2008, A comparison of imaging conditions for wave-equation shot-profile migration: Geophysics, **73**, S219-S227.

Valenciano, A., and B. Biondi, 2003, 2D deconvolution imaging condition for shot profile migration: 73rd Annual International Meeting, SEG, Expanded Abstracts, 1059-1062.

Versteeg, R., 1994, The Marmousi experience: Velocity model determination on a synthetic complex data set: The Leading Edge, **13**, 927-936.

Vivas, F. A., Pestana, R. C., and Ursin, B., 2009, A new stabilized least-squares imaging condition: Journal of Geophysics and Engineering, **6**, 264-268.